CENTER FOR CONNECTED AND AUTOMATED TRANSPORTATION

CCAT-CTS 25-14
November 2025

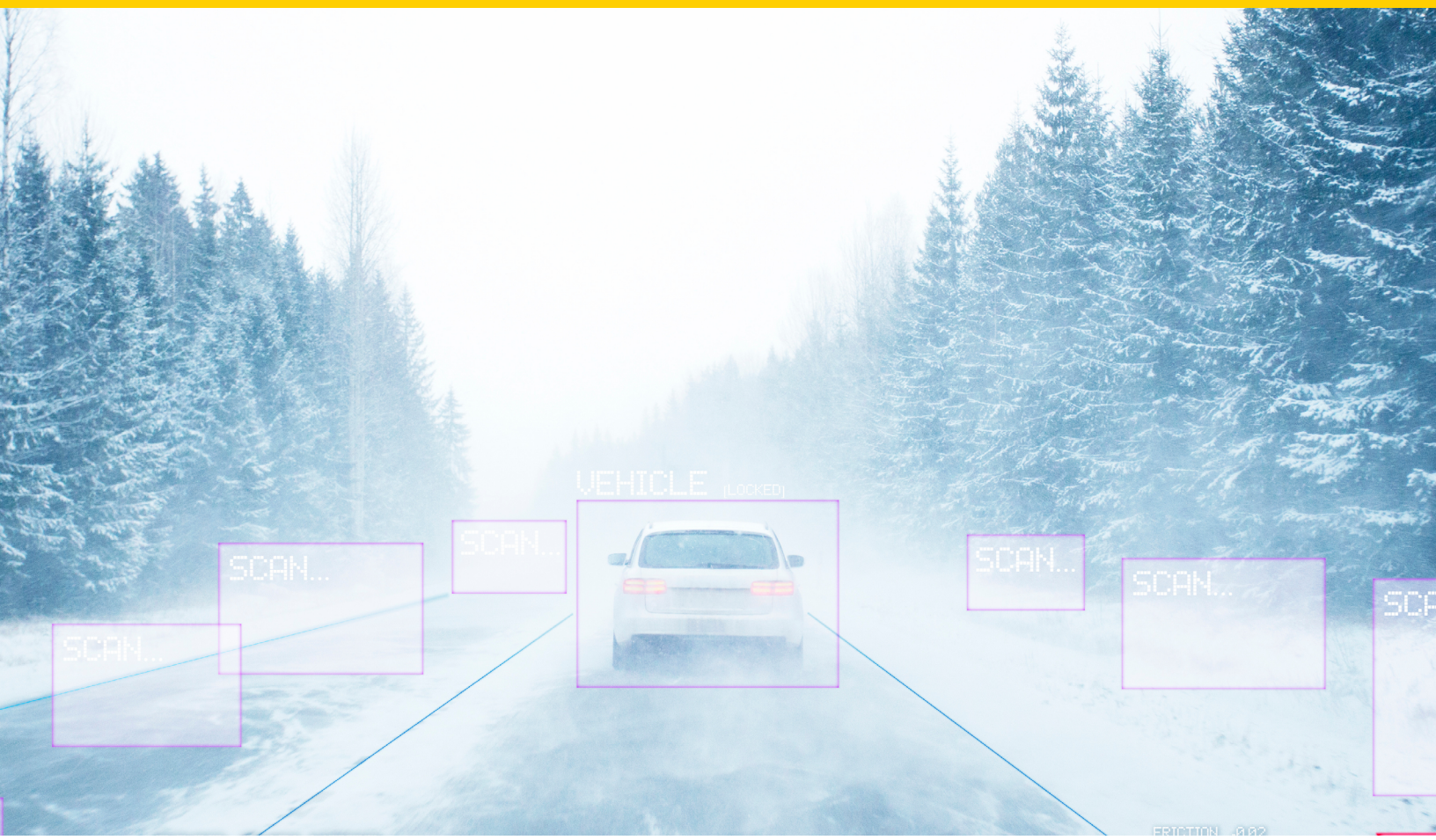

Autonomous Vehicle Challenges for the US Rural Midwest

Rajesh Rajamani
Hamidreza Alai
Gaurav Sharma
Hongjoon Kyong
Navaneeth Pushpalayam

Center for Transportation Studies

CENTER FOR CONNECTED AND AUTOMATED TRANSPORTATION

Report No. CTS 25-14

November 2025

Project Start Date: December 1, 2023

Project End Date: August 31, 2025

Autonomous Vehicle Challenges for the US Rural Midwest

by

Rajesh Rajamani

Hamidreza Alai

Gaurav Sharma

Hongjoon Kyong

Navaneeth Pushpalayam

University of Minnesota

CENTER FOR CONNECTED AND AUTOMATED TRANSPORTATION

DISCLAIMER

Funding for this research was provided by the Center for Connected and Automated Transportation under Grant No. 69A3551747105 of the U.S. Department of Transportation, Office of the Assistant Secretary for Research and Technology (OST-R), University Transportation Centers Program. The contents of this report reflect the views of the authors, who are responsible for the facts and the accuracy of the information presented herein. This document is disseminated under the sponsorship of the Department of Transportation, University Transportation Centers Program, in the interest of information exchange. The U.S. Government assumes no liability for the contents or use thereof.

Suggested APA Format Citation: Rajamani, R., Alai, H., Sharma, G., Kyong, H., Pushpalayam, N. (2025). Autonomous Vehicle Challenges for the Rural Midwest. Final Report.

Contacts

For more information:

University of Minnesota
Rajesh Rajamani
111 Church Street SE
Minneapolis, MN 55455
Phone: (612) 626-7961
Email: rajamani@umn.edu

CCAT
University of Michigan Transportation Research Institute
2901 Baxter Road
Ann Arbor, MI 48152
umtri-ccat@umich.edu
(734) 763-2498

CENTER FOR CONNECTED AND AUTOMATED TRANSPORTATION

Technical Report Documentation Page

1. Report No. CTS 25-14	**2. Government Accession No.**	**3. Recipient's Catalog No.**
4. Title and Subtitle **Autonomous Vehicle Challenges for the US Rural Midwest**		**5. Report Date** October 31, 2025 **6. Performing Organization Code** University of Minnesota
7. Author(s) Rajesh Rajamani, Ph.D. https://orcid.org/0000-0001-9931-7419 Hamidreza Alai, Ph.D. https://orcid.org/0009-0004-8105-2837 Gaurav Sharma https://orcid.org/0000-0001-5696-451X Hongjoon Kyong https://orcid.org/0000-0003-1581-4827 Navaneeth Pushpalayam https://orcid.org/0009-0001-5458-7594		**8. Performing Organization Report No.**
9. Performing Organization Name and Address Center for Connected and Automated Transportation University of Michigan Transportation Research Institute 2901 Baxter Road Ann Arbor, MI 48109 University of Minnesota 111 Church Street SE, Minneapolis, MN 55455.		**10. Work Unit No.** **11. Contract or Grant No.** Contract No. 69A3551747105
12. Sponsoring Agency Name and Address U.S. Department of Transportation Office of the Assistant Secretary for Research and Technology 1200 New Jersey Avenue, SE Washington, DC 20590		**13. Type of Report and Period Covered** Final Report (December 2023 – August 2025) **14. Sponsoring Agency Code** OST-R
15. Supplementary Notes Conducted under the U.S. DOT Office of the Assistant Secretary for Research and Technology's (OST-R) University Transportation Centers (UTC) program.		

UMTRI · The University of Akron · Central State University · Illinois Center for Transportation · University of Minnesota · Northwestern · Purdue University · Washtenaw Community College · Wisconsin – University of Wisconsin-Madison

CENTER FOR CONNECTED AND AUTOMATED TRANSPORTATION

16. Abstract

Low volume rural roads present special challenges for AVs, since they can be narrow, often will not have right-side lane markers, may not even have center lines, and may not be plowed for snow removal. Rural traffic intersections can have missing delineation and signage that are normally provided on higher volume roadways. All of these issues pose major challenges to autonomous driving. This project specifically looks into solutions for localization on rural roads without the use of cameras so that they can work in the absence of lane markers and/or in the presence of snow. The use of RTK-corrected GNSS is explored in detail. A full-scale Chrysler Pacifica MnCAV vehicle at the University of Minnesota was utilized for all data collection. On rural roads without obstructions from trees, RTK-corrected GNSS was found to yield better than 10 cm localization accuracy in terms of standard deviation of error. More than 20 satellites are typically available for use in the real-time position calculation on such roads. However, on roads with dense tree cover, satellite visibility may be completely lost on occasions.

The use of Lidar for localization by utilizing an open-source LIO-SAM algorithm was also explored in the project and the results obtained suggest that pre-made maps rather than a SLAM algorithm are needed for reliable localization with Lidar. Since a dual-antenna GNSS system equipped with a high performance IMU can cost well over $15,000, the feasibility of reliably estimating yaw angle and slip angle without the need for an expensive dual-antenna sensor was studied. Two novel approaches, one based on the use of a high gain observer that utilizes IMU and single-antenna GNSS measurements, and another based on the use of a low-cost radar on the car, were developed. Both approaches showed very good performance with yaw angle and slip angle estimates being within approximately 1 degree of ground truth readings.

The results obtained in this project indicate that a low-cost single-antenna GNSS system can work reliably for localization on rural roads that have at least some open-sky visibility (don't have dense tree cover).

17. Key Words	18. Distribution Statement		
Autonomous driving, GNSS, automated steering, localization	No restrictions.		
19. Security Classif. (of this report)	**20. Security Classif. (of this page)**	**21. No. of Pages**	**22. Price**
Unclassified	Unclassified	33	Leave blank – not used

Form DOT F 1700.7 (8-72) Reproduction of completed page authorized

UMTRI | The University of Akron | Central State University | Illinois Center for Transportation | University of Minnesota | Northwestern | Purdue University | Washtenaw Community College | Wisconsin – University of Wisconsin-Madison

Abstract

About 75% of all roads in the United States, around 3 million miles, are in rural areas and are vital for transporting goods and connecting communities. The risk of dying in a car crash is 62% higher on a rural road compared to an urban road for trips of the same length. Locally, in the state of Minnesota, nearly two-thirds of all crashes leading to fatalities or serious injuries occur at rural intersections. Since a vast majority of these crashes occur due to human error, autonomous vehicles (AVs) have the potential to improve rural road safety. However, low volume rural roads present special challenges for AVs. Such rural roads can be narrow, often will not have right-side lane markers, may not even have center lines, may not be plowed for snow removal, and can have trees and other objects close to the side of the road. Rural traffic intersections can have missing delineation and signage that are normally provided on higher volume roadways. All of these issues pose major challenges to autonomous driving.

This project specifically looks into solutions for localization on rural roads without the use of cameras so that they can work in the absence of lane markers and/or the presence of snow. The use of RTK-corrected GNSS is explored in detail. The full-scale Chrysler Pacifica MnCAV vehicle at the University of Minnesota was utilized for all data collection. On rural roads without obstructions from trees, RTK-corrected GNSS was found to yield better than 10 cm localization accuracy in terms of standard deviation of error. More than 20 satellites are typically available for use in the real-time position calculation on such roads. However, on roads with dense tree cover, satellite visibility may be completely lost – Data collected on a narrow suburban road with dense trees showed GNSS dropouts lasting several seconds on multiple occasions.

The use of Lidar for localization by utilizing an open-source LIO-SAM algorithm was explored. This algorithm is a state-of-the-art computational framework that is designed to provide real-time trajectory estimation and map-building for autonomous systems like robots and self-driving vehicles. By using the Lidar sensor to measure distances to the surrounding environment and performing a process called scan-matching, where consecutive Lidar scans are aligned to estimate how far the vehicle has moved between scans, the new location of the vehicle is determined. Analysis of data from the MnCAV vehicle with this algorithm showed that position drifts of approximately 0.2m, 0.5 m and 0.8 m are obtained when GNSS outages occur of 1, 5 and 10 seconds respectively. These results suggest that pre-made maps rather than a SLAM algorithm are needed for reliable localization with Lidar.

Since a dual-antenna GNSS system equipped with a high performance IMU can cost well over $15,000, the feasibility of reliably estimating yaw angle and slip angle without the need for an expensive dual-antenna sensor was studied. Two novel approaches, one based on the use of a high gain observer that utilizes IMU and single-antenna GNSS measurements, and another based on the use of a low-cost radar on the car, were developed. Both approaches showed very good performance with yaw angle and slip angle estimates being within approximately 1 degree of ground truth readings.

The results obtained in this project indicate that a low-cost single-antenna GNSS system can work reliably for localization on rural roads that have at least some open-sky visibility (don’t have dense tree cover).

Table of Contents

1. Introduction

Crashes on Rural Roads

About 75% of all roads in the United States, around 3 million miles, are in rural areas and are vital for transporting goods and connecting communities. The likelihood that a car crash will result in death is higher in rural America, even with less than one fifth of the population living in these areas [1]. Approximately 85,000 people were killed on rural roads between 2016 and 2020. According to a new study published by the Governors Highway Safety Association (GHSA), the risk of dying in a car crash was 62% higher on a rural road compared to an urban road for trips of the same length [1]. Locally, in the state of Minnesota, nearly two-thirds of all crashes leading to fatalities or serious injuries occur at rural intersections. More than 20% of all traffic fatalities in the United States occur at intersections, and over 80% of intersection-related fatalities in rural areas occur at unsignalized intersections [2].

Challenges for Rural Autonomous Driving

While major global companies such as Google, Uber, Tesla and General Motors are intensively focused on developing Level 3 and higher self-driving autonomous vehicles, their research is focused on driving in good weather on clean well-equipped roads. A majority of their development and testing has occurred in warm weather states such as California and Arizona. States in the US Midwest and rural locations pose additional challenges for autonomous driving that could significantly delay the arrival of self-driving technology to these regions.

The use of cameras is the most common approach for determining a vehicle's position in the lane and for measuring its lateral distance with respect to the lane boundaries. This lateral distance to lane markers is used as the feedback variable for automatic steering control [3]. The presence of snow on the ground, including even a thin layer of frost covering the lane markers, can make the engagement of steering control infeasible. Data gathered by the University of Minnesota team shows that snow remains on lane markers for a significantly longer duration, compared to snow in the interior of the lane where the tire-paths of cars enable faster snow removal. This prevents the engagement of autonomous steering for a significant period of time after the end of snowfall. Further, low volume rural roads present special challenges in all seasons. Such rural roads can be narrow, often will not have right-side lane markers, may not even have center lines, may not be plowed for snow removal, and can have trees and other objects close to the side of the road. Rural traffic intersections can have missing delineation and signage that are normally provided on higher volume roadways. All of these issues pose major challenges to autonomous driving, since AVs depend critically on such markings and signage.

Level-2 vehicles with automatic steering control for lane centering currently sold in the market rely on camera-based feedback [3]. The use of differential GPS (as an alternative to camera-based feedback) for steering control was pioneered by researchers at the University of Minnesota [4] and has also been studied by researchers at other universities and companies [5]. The differential GPS system reported in these early papers was typically an expensive local system

created specifically for the research project under consideration. A description of dynamic models for representing lateral vehicle motion and of automatic steering control systems can be found in [6], [7]. The use of the state-wide MnCORS GNSS network in Minnesota for providing RTK corrections for lateral lane position measurement has been utilized by Davis, et al for a snowplow guidance system that approximately detects lateral position and displays it with a resolution of 1 foot inside the snowplow cab [8], [9].

Project Objectives

This project will explore some solutions to the challenges associated with rural driving for autonomous vehicles. In particular, the project will explore the use of RTK-corrected GNSS for localization of the autonomous vehicle so that the vehicle can then perform steering control using such GNSS-based measurements instead of traditional camera-based relative position measurements with respect to lane boundaries. The availability and accuracy of GNSS-based measurements in rural environments will be studied. Estimation approaches that can reduce the cost of GNSS device hardware will be explored. Alternative Lidar-based localization techniques that can compensate for GNSS outages will also be considered.

MnCAV Vehicle Summary

This section provides a brief summary of the University of Minnesota's autonomous vehicle, known as the MnCAV vehicle, as shown in the photograph in Figure 1. The vehicle is equipped with RTK corrected GPS, IMU, gyroscope and radar and their specifications are given in Table 1. The vehicle belongs to the Center for Transportation Studies at the University of Minnesota. The project will utilize this vehicle for all of the data collection tasks that will be performed in various road environments.

Figure 1: Photograph of the University of Minnesota MnCAV automated vehicle (Credit: Center for Transportation Studies, University of Minnesota, https://mncav.umn.edu/)

The MnCAV vehicle is equipped with firmware for computer-controlled steering, throttle and brakes and is instrumented with sophisticated sensors that include high-density 3D Lidar, forward and rear facing radar, inertial measurement unit (IMU) sensors, dual antenna GPS system capable of obtaining RTK corrections from MnCORS, a Mobileye Camera system for measuring distances from lane boundaries, and multiple other cameras for recording of the road environment and of the motions of other nearby vehicles.

Table 1: Sensor Specifications

Sensor	Accuracy	Rate (Hz)
Novatel PWRPAK7-E2 GPS	10 cm	10
Accelerometer	0.025 m/s/√hr	100
Gyroscope	0.06 °/√hr	100
CONTI ARS408 Radar	10 cm	20
Ouster OS1-64 Lidar	5 cm	10

Figure 2(a) shows the Novatel PwrPak7D-E1 module used on the MnCAV vehicle for GNSS based position measurement. Figure 2(b) shows the MnCAV vehicle equipped with a dual antenna system that interfaces with the Novatel GNSS module. The Novatel module supports dual antenna receivers and RTK corrections communicated over multi-channel L-band and IP connections. The left antenna is the primary antenna or the main GNSS antenna used for position determination. The right antenna is the secondary antenna and is used to obtain a high-accuracy orientation angle of the vehicle.

(a) Novatel PwrPak7D-E1 module

(Available at: https://novatel.com/products/gnss-inertial-navigation-systems/combined-systems/pwrpak7d-e1)

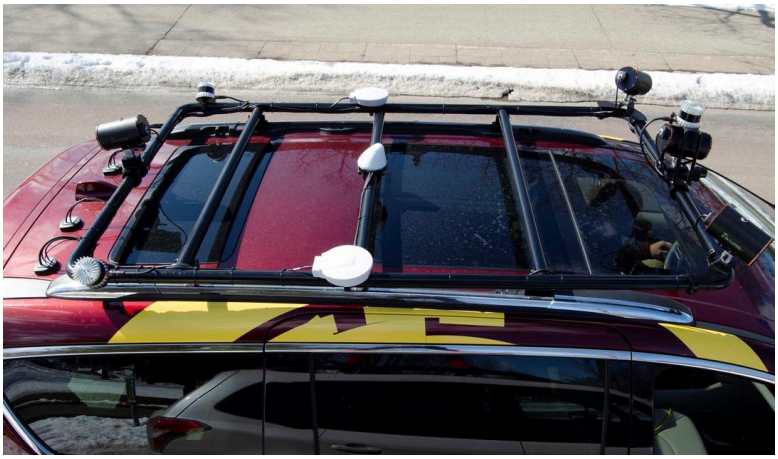

(b) MnCAV vehicle with roof-equipped dual GNSS antenna system

(Credit: Center for Transportation Studies, University of Minnesota, https://mncav.umn.edu/)

Figure 2: GNSS Module and dual antenna system used on the MnCAV vehicle

2. GNSS Availability in Rural Environments

The project first focused on preliminary data collection using the MnCAV autonomous vehicle to analyze the availability and accuracy of GNSS (global navigation satellite system) based position measurements for autonomous steering control. The MnCORS RTK (real-time kinematic) correction system was utilized to increase GNSS position estimation accuracy. Data was obtained on a variety of roads, including rural roads without blockage from trees, roads in downtown Minneapolis, non-downtown/ suburban roads without tree cover and suburban roads with tree cover. This section presents a summary from the analysis of satellite availability and position measurement accuracy at these different locations.

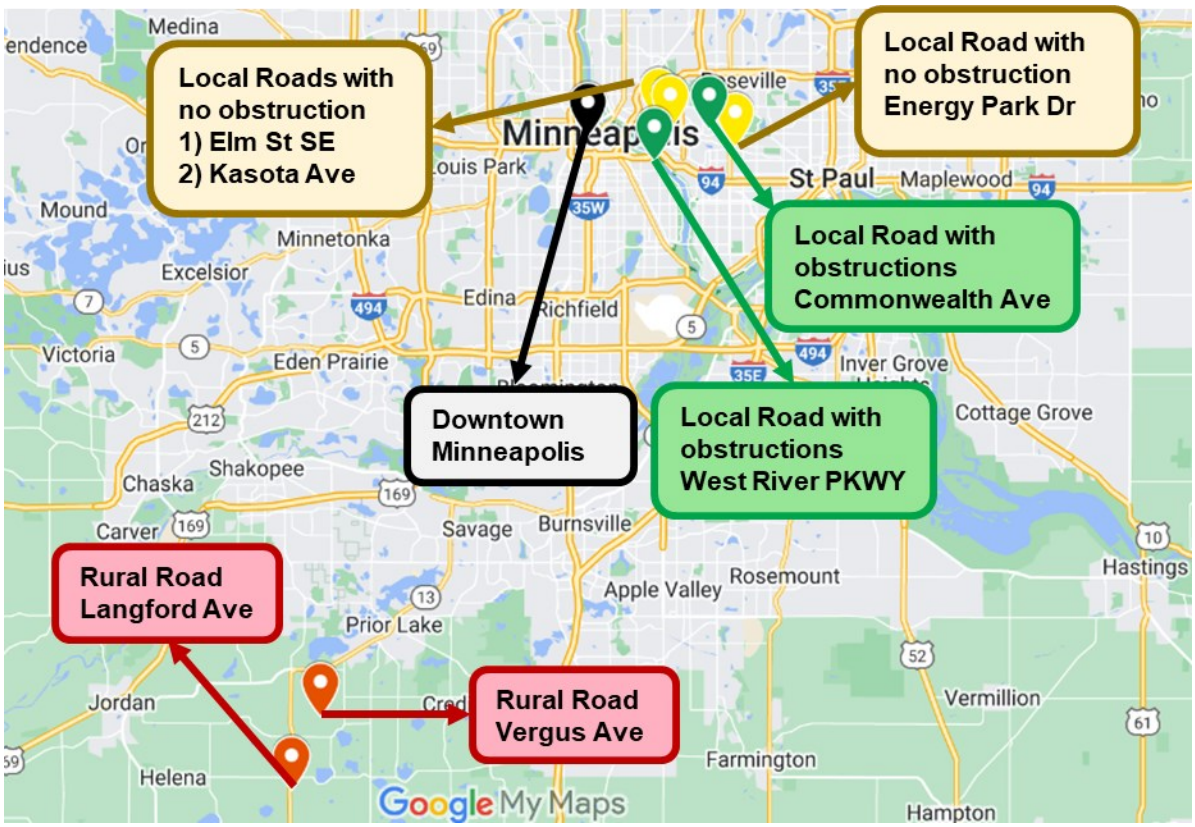

Figure 3: Map showing roads at a variety of locations used for testing the GNSS system

Figure 3 shows a variety of locations at which the performance of the GNSS system with RTK corrections from MnCORS was tested. The locations include a rural main road (Langford Ave), a rural side road (Vergus Ave), downtown Minneapolis, local non-downtown roads near campus with no obstructions (Elm St SE, Kasota Ave, Energy Park Drive) and local non-downtown roads with some tree obstructions (West River Parkway and Commonwealth Ave). Additional data collection at more rural locations needs to be conducted in the future to further confirm the results from this preliminary analysis.

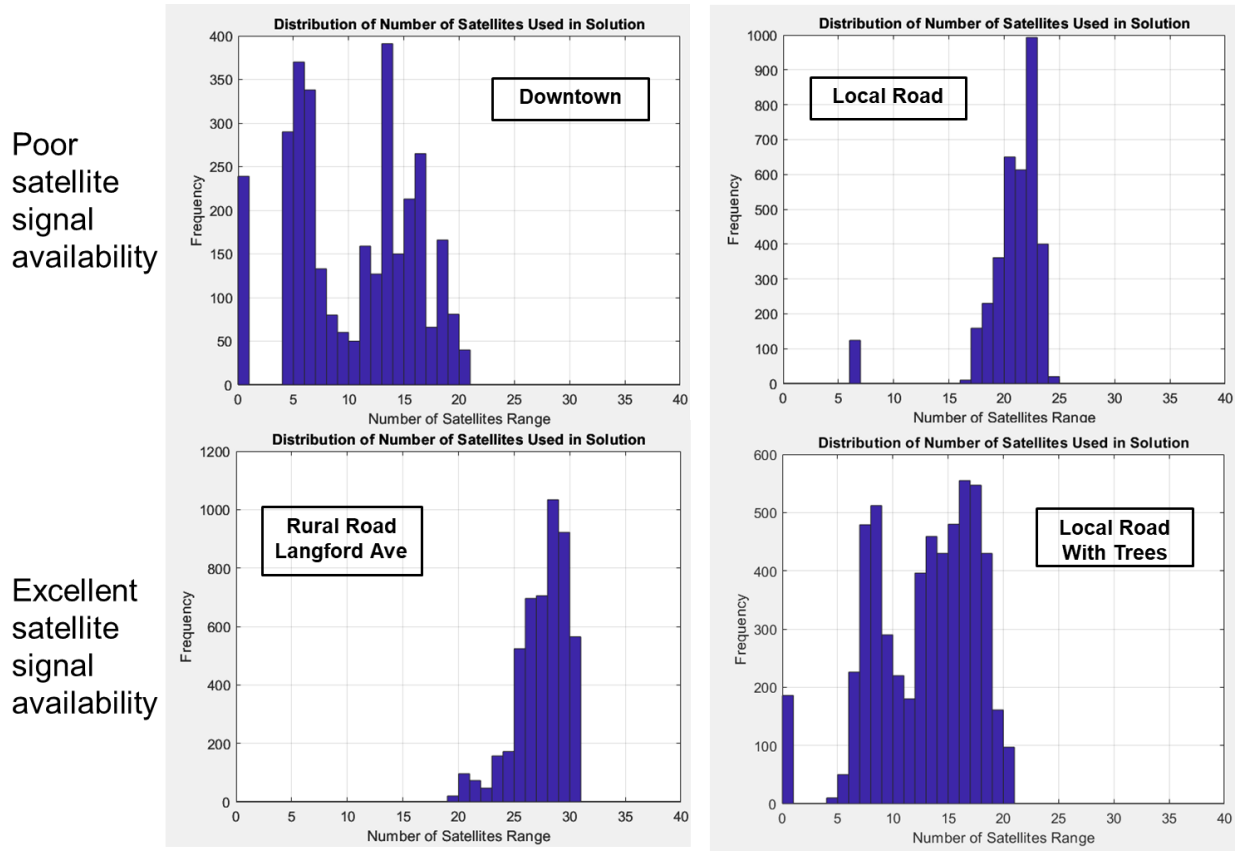

Figure 4: Satellite availability characterization of various locations

Figure 4 shows a characterization of the number of satellites available for position determination at each of 4 characteristic locations: downtown Minneapolis, a rural main road, a local non-downtown road without obstructions and a local non-downtown road with tree obstructions. From the results in Figure 4, it can be seen that

- Due to the many tall buildings and skyways in downtown Minneapolis, the number of satellites used in position determination drops to very small numbers in many instances. There were 240 instances (each lasting 0.1 seconds) when there were less than 4 satellites visible and hence position could not be determined at all.
- On Langford Ave (a rural main road), there are not much trees to obstruct the lines of sight to satellites. Therefore, there was a large number of satellites ($\geq$ 20) always available to be used in the position determination solution.
- On suburban local roads with obstructions, the number of satellites used in the position determination solution is smaller than on roads with no obstruction, but more than in downtown where the case is significantly worse.
- On suburban local roads with no obstructions, the number of satellites available to be used in solution is very good (and always adequate to prevent loss of position determination).

Figure 5 shows a characterization of the predicted standard deviation in longitude position measurement at the 4 characteristic locations. It can be seen that the rural road (Langford Ave) always has excellent position accuracy with the predicted standard deviation always being less than 10 cm. On the other hand, the downtown test has many instances of poor position accuracy in which the standard deviation increases significantly and can be well over 1 meter. The local road with no obstructions has good accuracy with standard deviation being less than 10 cm for most readings. The local road with tree obstructions has several instances of loss in accuracy wherein the standard deviation can increase to over 1 meter, although the accuracy is significantly better than that of downtown most of the time.

Many instances of poor accuracy

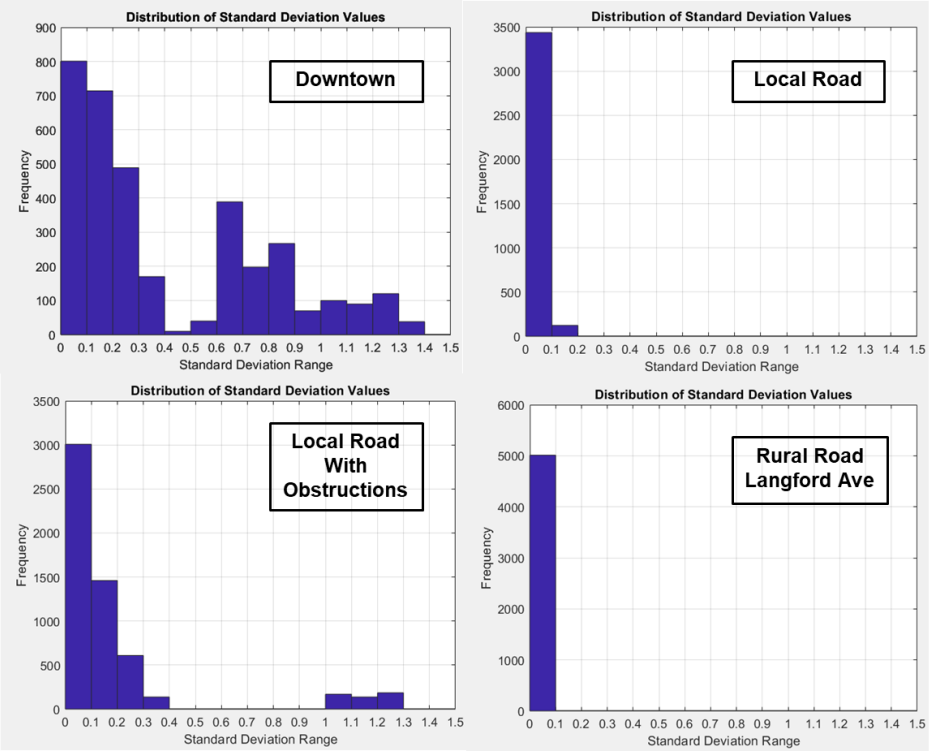

Always excellent accuracy

Figure 5: Standard deviation of longitude measurement at various locations

Figure 6 shows a similar characterization of the predicted standard deviation in latitude position measurement at the 4 characteristic locations. The conclusions from this figure are identical to the ones from Figure 5.

A detailed analysis of whether the brief GNSS outages can be handled by IMU based integration methods remains to be done and was not taken up as a part of this CCAT project.

Many instances of poor accuracy

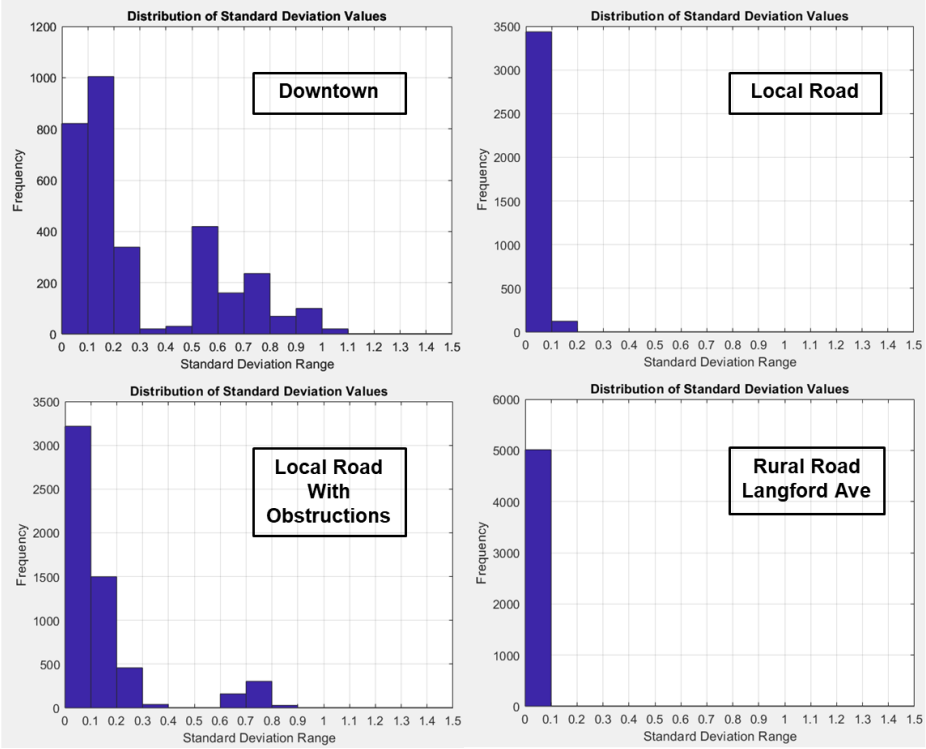

Always excellent accuracy

Figure 6: Standard deviation of latitude measurement at various locations

From all of the data we have collected so far, the standard deviation appears to be 10 cm or better on rural roads and local roads without obstructions where the number of satellites available is typically more than 15.

Figure 7 shows the availability (or accuracy) of RTK corrections in determining positions at the same 4 characteristic locations. It can be seen that RTK corrections were not available for approximately 40% of the time in the downtown test (Here *availability* actually refers to accuracy of the RTK correction and such accuracy is compromised by multipath errors). Since RTK correction is susceptible to multipath errors which occur frequently in the presence of tall buildings, RTK correction can often be unavailable in downtown, as evidenced by the results of Figure 6. RTK corrections were available almost 100% of the time in the rural location and local road without obstruction tests. In the case of the local road with tree cover, RTK corrections were not available approximately 20% of the time.

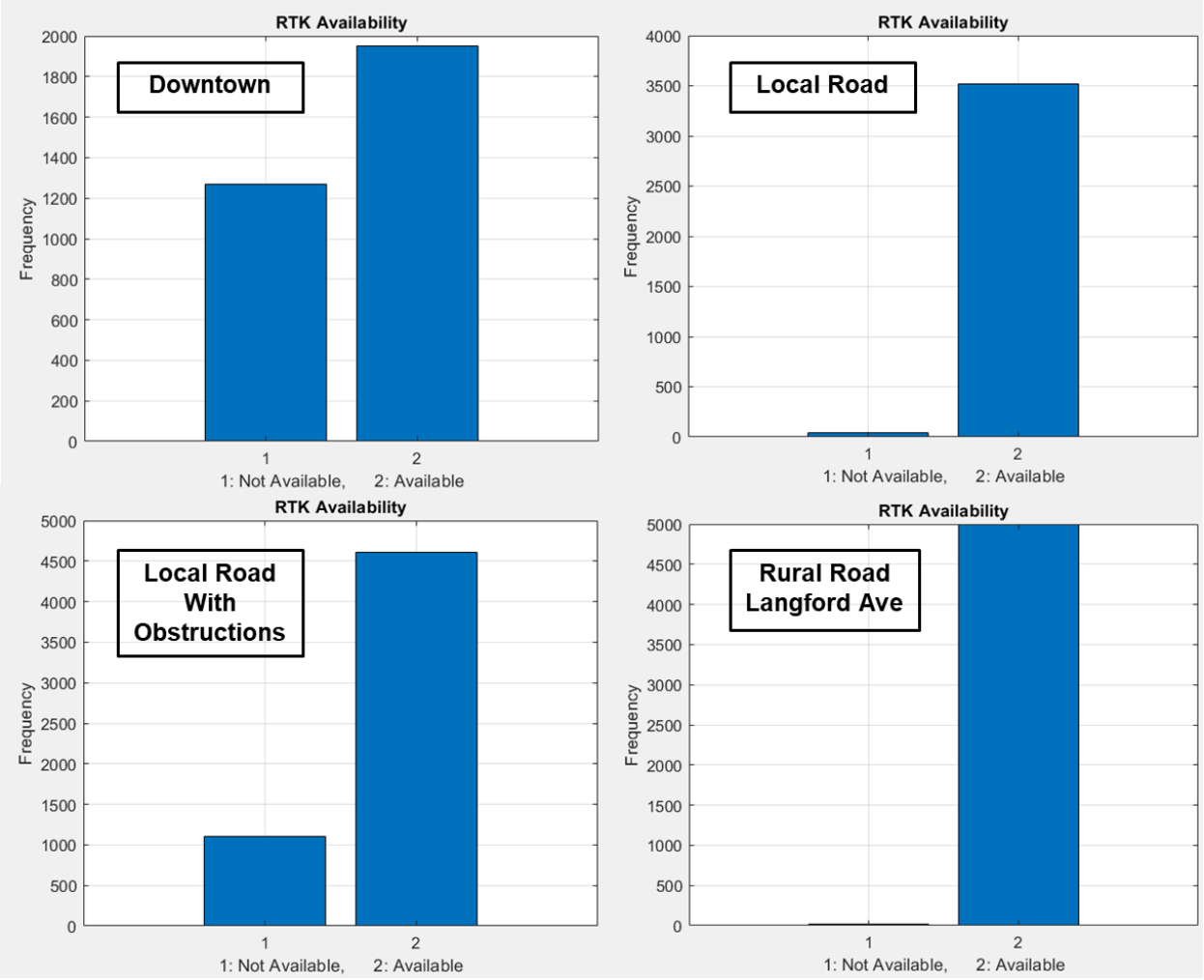

Figure 7: RTK correction availability characterization at various locations

Alternate Methods to Estimate Yaw Angle and Slip Angle

A dual-antenna GNSS system equipped with a high performance IMU sensor can cost well over $15,000. For example, the Novatel PwrPak7D-E1 module utilized on the MnCAV vehicle had a cost of over $17,500 when initially purchased (~in 2022). The use of a single-antenna device together with the use of a low-cost IMU can significantly reduce hardware costs. This section explores the development of alternate techniques for estimating yaw angle and slip angle so that the use of a dual antenna system can be avoided. The yaw angle of the vehicle is needed for autonomous steering control, since the yaw error between the road and the vehicle, as well as the look-ahead lateral position error, need to be used in the feedback control system. Two approaches are studied for yaw and slip angle estimation:

A) A high gain observer based yaw and slip angle method in which IMU measurements are used as inputs to a process dynamics model, in addition to measurements from a single-antenna GNSS system.

B) A radar based method in which radial distances and velocities with respect to static objects on the road can be utilized for slip angle (and consequently yaw angle) estimation. Radar is typically already utilized on all autonomous vehicles for object detection and tracking tasks and is thus a sensor that is already available on the vehicle.

3. High Gain Observer Based Yaw and Slip Angle Estimation

Consider the state vector for an autonomous vehicle's ego state estimation,

$$z_E = [x_E \quad \dot{x}_E \quad \ddot{x}_E \quad y_E \quad \dot{y}_E \quad \ddot{y}_E]^T = [z_1 \quad \dots \quad z_6]^T \tag{1}$$

The acceleration of the ego vehicle in the inertial frame is given by,

$$\ddot{x}_E = a_x \cos(\psi_E) - a_y \sin(\psi_E) \tag{2}$$

$$\ddot{y}_E = a_x \sin(\psi_E) + a_y \cos(\psi_E) \tag{3}$$

where, a_x and a_y are the acceleration of the ego vehicle about inertial X_E and Y_E axis obtained which can be obtained using an IMU.

The jerk of the ego vehicle in the inertial frame is the derivative of (2) and (3) which is given as follows,

$$\dddot{x}_E = \dot{a}_x \cos(\psi_E) - \dot{a}_y \sin(\psi_E) - u_3 \dot{y}_E \tag{4}$$

$$\dddot{y}_E = \dot{a}_x \sin(\psi_E) + \dot{a}_y \cos(\psi_E) + u_3 \ddot{x}_E \tag{5}$$

where, $\dot{a}_x$ and $\dot{a}_y$ are the derivative of the IMU readings and u_3 is the yaw rate obtained from the gyroscope. The IMU and gyroscope signal derivatives $\dot{a}_x, \dot{a}_y$ and $\dot{u}_3$ cannot be measured directly and moreover the differentiation of IMU readings will yield highly noise values, hence it has been assumed that these derivatives are zero.

Assumption 1. The jerk (derivative of acceleration and angular acceleration) is zero: $\dot{a}_x = 0$, $\dot{a}_y = 0$ and $\dot{u}_3 = 0$.

Given the above assumption, (4) and (5) can be simplified as follows,

$$\dddot{x}_E = -u_3 \dot{y}_E \tag{6}$$

$$\dddot{y}_E = u_3 \ddot{x}_E \tag{7}$$

The new state dynamics is then given as follows,

$$\dot{z}_E = F z_E + G f_E(u_3, z_E) \tag{8}$$

where, $F = \begin{bmatrix} 0 & 1 & 0 & 0 & 0 & 0 \\ 0 & 0 & 1 & 0 & 0 & 0 \\ 0 & 0 & 0 & 0 & 0 & 0 \\ 0 & 0 & 0 & 0 & 1 & 0 \\ 0 & 0 & 0 & 0 & 0 & 1 \\ 0 & 0 & 0 & 0 & 0 & 0 \end{bmatrix}$,

$G = \begin{bmatrix} 0 & 0 \\ 0 & 0 \\ 1 & 0 \\ 0 & 0 \\ 0 & 0 \\ 0 & 1 \end{bmatrix}$ and $f_E(u_3, z_E) = \begin{bmatrix} f_1(u_3, z_E) \\ f_2(u_3, z_E) \end{bmatrix} = \begin{bmatrix} -u_3 z_6 \\ u_3 z_3 \end{bmatrix}$.

The measurement equation is then given by,

$$y = Hz_E \tag{9}$$

where $H = \begin{bmatrix} 1 & 0 & 0 & 0 & 0 & 0 \\ 0 & 0 & 0 & 1 & 0 & 0 \end{bmatrix}$.

It can be observed that accurate state estimates can be obtained from the use of just GPS positions and gyroscope measurements when assumption 1 is satisfied, without using the IMU accelerations.

After obtaining the companion form for state estimation of ego vehicle, the observer dynamics as can be obtained as follows,

$$\dot{\hat{z}}_E = F\hat{z}_E + Gf_E(u_3, \hat{z}_E) + L_E(y - H\hat{z}_E) \tag{10}$$

where L_E is the constant observer gain matrix. It is assumed that the nonlinear process equation is Lipschitz,

$$\left\|\tilde{f}_E\right\|_2 \leq \gamma \|\tilde{z}_E\|_2 \tag{11}$$

where, $\tilde{f}_E = f(u_3, z_E) - f(u_3, \hat{z}_E)$ and $\tilde{z}_E = z_E - \hat{z}_E$ and γ is the Lipschitz constant and for state estimation it is given by the maximum angular velocity encountered during the motion of the ego vehicle i.e. $\gamma = u_3|_{max}$.

The high gain observer formulation requires the dynamics to be in the block triangular form as given in (8), after which the observer gain can be obtained by solving the LMI given in Theorem 1.

Theorem 1. If there exists $P > 0$, $\lambda > 0$, L, and $\theta > 1$ such that:

$$F^T P + PF - H^T R - R^T H < -\lambda I \tag{12}$$

and

$$\theta > \theta_0 = \frac{2\gamma\lambda_{max}(P)}{\lambda} \tag{13}$$

in which $\lambda_{max}(.)$ is the maximum eigenvalue, then the estimation error $\tilde{z}$ is exponentially stable by taking:

$$K = P^{-1}R^T \tag{14}$$

$$L = T(\theta)K \tag{15}$$

where, $T(\theta) = \begin{bmatrix} \theta & 0 & 0 & 0 & 0 & 0 \\ 0 & \theta^2 & 0 & 0 & 0 & 0 \\ 0 & 0 & \theta^3 & 0 & 0 & 0 \\ 0 & 0 & 0 & \theta & 0 & 0 \\ 0 & 0 & 0 & 0 & \theta^2 & 0 \\ 0 & 0 & 0 & 0 & 0 & \theta^3 \end{bmatrix}$, $\theta > 1$.

The proof of the above Theorem can be obtained from Gauthier, et al., 1994, [10].

After obtaining the ego state estimates z_E, it is very important to compute the yaw angle of the ego vehicle, which can be obtained as follows using (2) and (3),

$$cos(\psi_E) = \frac{a_x\ddot{x}_E + a_y\ddot{y}_E}{\sqrt{a_x^2 + a_y^2}} \tag{16}$$

The above equation can be used to estimate the yaw angle although it will not work for the case when the ego vehicle is not accelerating. In such cases the yaw angle can be approximated as the course angle γ_E which can be computed as follows,

$$\gamma_E = \psi_E + \beta_E = tan^{-1}\left(\frac{\dot{y}_E}{\dot{x}_E}\right) \tag{17}$$

Given the measurements in (16) and (17), the following observer can be used to estimate the yaw angle of the ego vehicle,

$$\dot{\hat{\psi}}_E = u_3 + k_1\left(y_1 - \hat{\psi}_E\right) + k_2(y_2 - \hat{\psi}_E) \tag{18}$$

where, $y_1 = tan^{-1}\left(\frac{\dot{y}_E}{\dot{x}_E}\right)$ and $y_2 = \cos^{-1}\left(\frac{a_x\ddot{x}_E + a_y\ddot{y}_E}{\sqrt{a_x^2 + a_y^2}}\right)$. The value of k_1 and k_2 can be decided based on the value of gyroscope reading or the accelerometer readings as follows,

If $u_3 > u_{th}$ then $k_1 = 0$ else $k_2 = 0$.

If $\sqrt{a_x^2 + a_y^2} > a_{th}$ then $k_1 = 0$ else $k_2 = 0$.

where, u_{th} and a_{th} are the threshold values of gyroscope or accelerometer respectively. Since at any point of time one of k_1 and k_2 will be present, the observer in (18) becomes,

$$\dot{\hat{\psi}}_E = u_3 + k_t\left(y_t - \hat{\psi}_E\right) \tag{19}$$

where $k_t = k_1$ or k_2 and $y_t = y_1$ or y_2 depending on the conditions on gyroscope or accelerometer readings. Both y_1 and y_2 will have some errors along with the gyroscope reading. Hence, the actual system for yaw angle estimation can be written as follows,

$$\dot{\psi}_E = u_3 + Bw \; and \; y_t = \psi_E + Dw \tag{20}$$

where, $w = [w_1 \quad w_2]^T$ and B and $D \in \mathbb{R}^{1\times 2}$.

The H_∞ disturbance rejection criteria can be used to obtain the observer gain k_t thus bounding the the error induced due to sensor noise for the system given in (38). Theorem 2 can be used to obtain the observer gain k_t.

Theorem 2. Consider the system in the form (20).

If there exists $k_t > 0$, $P > 0$, and $\mu > 0$ such that the following LMI is satisfied:

$$\begin{bmatrix} -2Pk + 1 & P(B - kD) \\ -(kD + B)^T P & -\mu I \end{bmatrix} \leq 0 \tag{21}$$

then the observer as given in (19) will be stable and a H_∞ disturbance rejection criterion will be satisfied.

Proof. Consider the Lyapunov candidate function,

$$V = \tilde{\psi}_E^2 P \tag{22}$$

where, $\tilde{\psi}_E = \psi_E - \hat{\psi}_E$ and $P > 0$. The derivative of V becomes,

$$\dot{V} = \tilde{\psi}_E^T P \dot{\tilde{\psi}}_E + \dot{\tilde{\psi}}_E^T P \tilde{\psi}_E = -2Pk\tilde{\Psi}_E^2 + P(B - k_t D)\tilde{\Psi}_E w + (B - kD)^T P \tilde{\Psi}_E w^T \tag{23}$$

Using the H_∞ disturbance rejection criteria (Zemouche & Boutayeb, 2009),

$$\dot{V} + ||\tilde{\psi}_E||^2 - \mu||w||^2 \leq 0 \tag{24}$$

Using (22), (23) can be written in matrix form as follows,

$$\begin{bmatrix} \tilde{\Psi}_E & w^T \end{bmatrix} \begin{bmatrix} -2Pk + 1 & P(B - kD) \\ (-kD + B)^T P & -\mu I \end{bmatrix} \begin{bmatrix} \tilde{\Psi}_E \\ w \end{bmatrix} \leq 0 \tag{25}$$

The solution of (24) results in solving the LMI as given in (21) and hence the proof is complete. ■

The complete flow chart for ego vehicle state estimation is given in Figure 8.

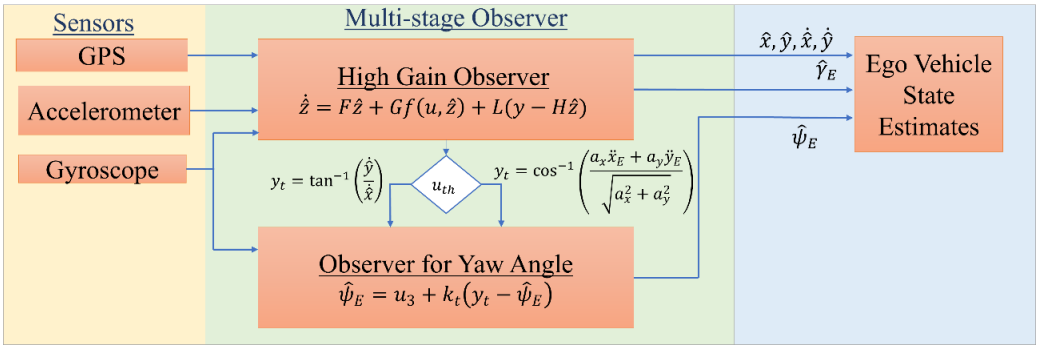

Figure 8: Multi-stage high gain observer for state estimation of ego vehicle.

This section provides the experimental results for state estimation and vehicle tracking obtained using the University of Minnesota's autonomous vehicle MnCAV. The vehicle is equipped with RTK corrected GPS, IMU, gyroscope and radar and their specifications are given in Table 1. The GPS position, gyroscope and IMU readings of the MnCAV vehicle were used as measurements for the ego vehicle state estimation by which the inertial position, yaw and course angle of the ego vehicle was estimated. The inputs from the ego state estimates were then utilized by vehicle tracking algorithms along with the radar readings of the tracked vehicle which was obtained from the Continental ARS408 Radar sensor. The tracked position, velocity, course and yaw angle obtained from the vehicle tracking algorithm were then compared with the ground truth data of the tracked vehicle obtained using MATLAB ground truth labeler using the highly accurate Ouster OS1-64 Lidar mounted on the Ego vehicle. The tracking algorithms developed in this work utilize some variables from the sensors (which includes the position of the ego and tracked vehicle, along with the acceleration and yaw rate of ego vehicle) to estimate many other variables (which includes the yaw angle, course angle and the velocities of the ego and tracked vehicles). The performance of the developed observer was evaluated using the error in estimation of V_C, V_{rel} and γ_C where $V_{rel} = \sqrt{\dot{r}_x^2 + \dot{r}_y^2}$ and γ_C is the course angle of the target vehicle.

To effectively evaluate the ego vehicle state estimation, tests were performed for a curved road in a parking lot at the University of Minnesota as shown in Figure 9. The plot for the position, yaw angle and side slip angle are shown in Figure 10 and it can be seen that the observer is able to estimate all these variables accurately. Furthermore, even the side slip angle is being estimated accurately over both straight road and curved path when the actual side slip is large. Additional estimation results for a second experiment are presented in Figure 11 and Figure 12.

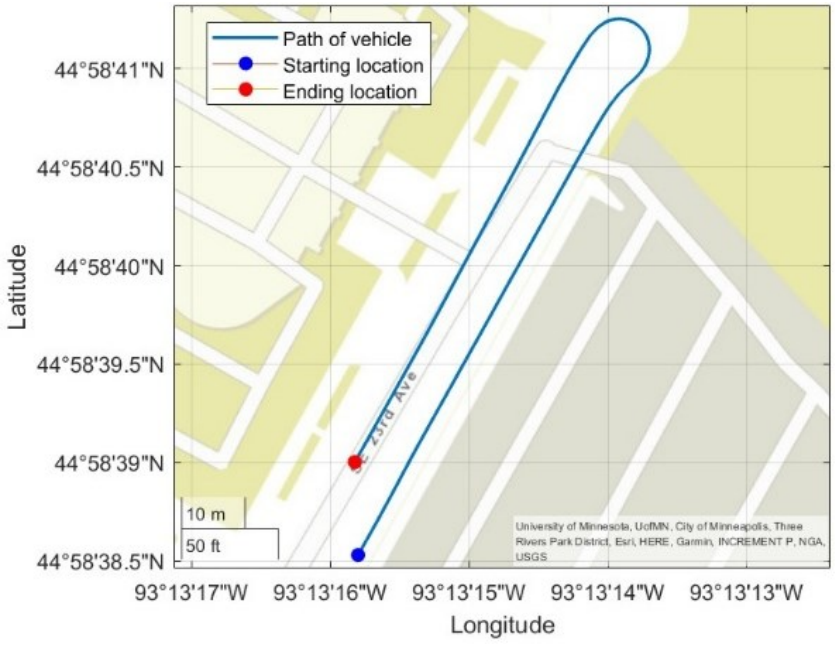

Figure 9: Route 1 of autonomous during state estimation.

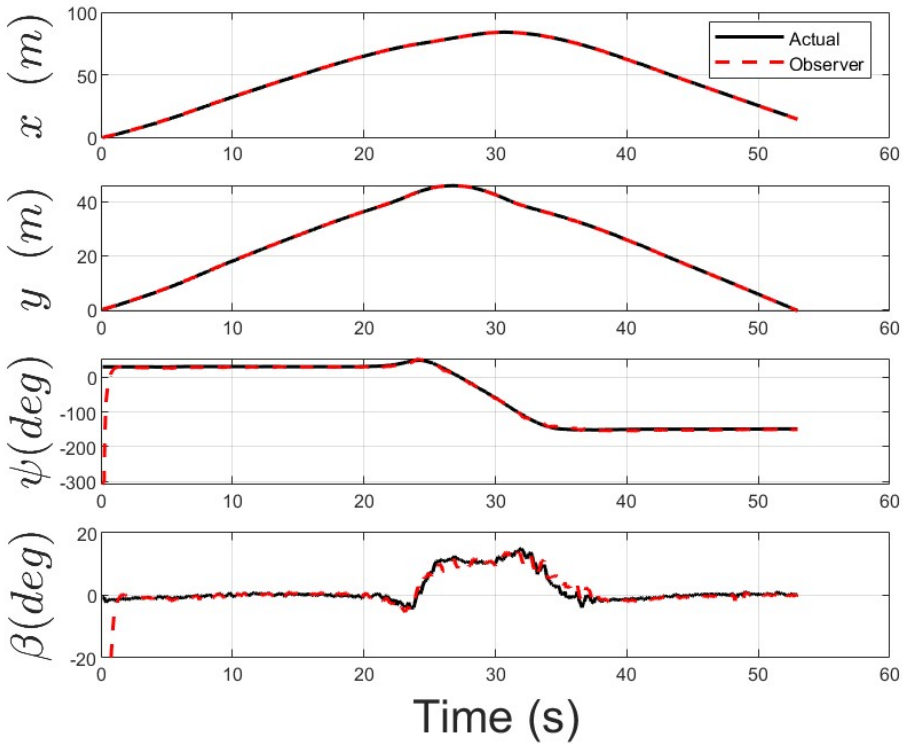

Figure 10: State estimation of ego vehicle on route 1.

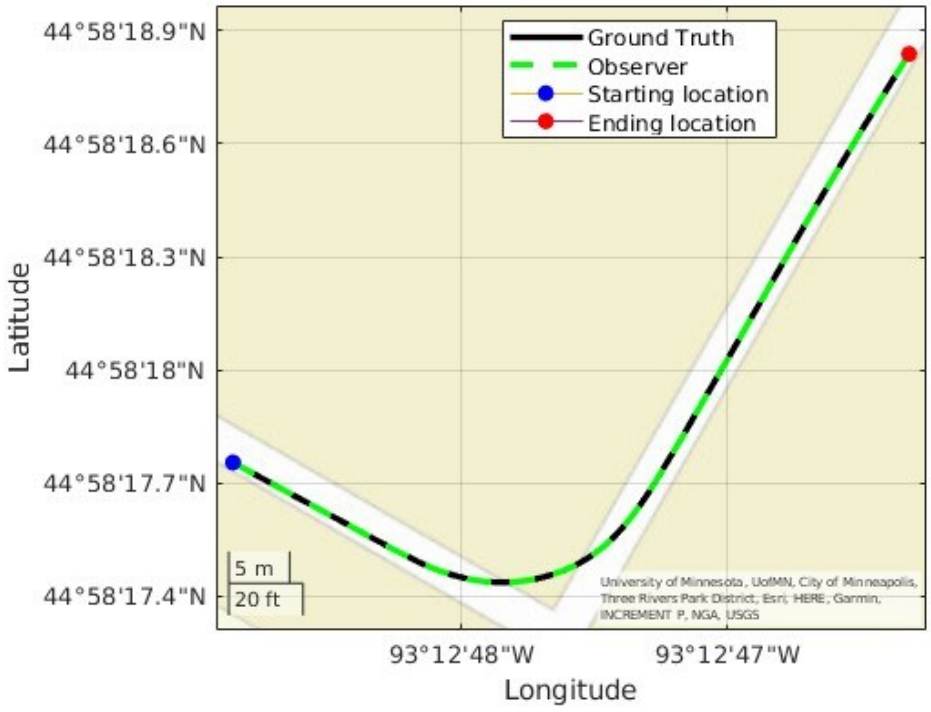

Figure 11: Route 2 of autonomous vehicle during state estimation.

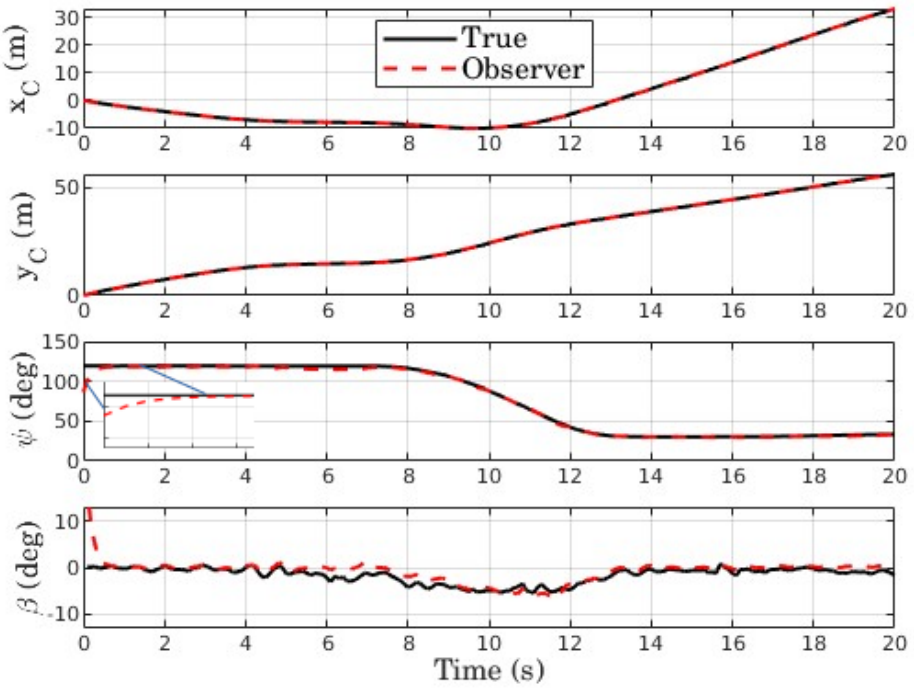

Figure 12: State estimation of ego vehicle on route 2.

4. Slip Angle Estimation Using On-Board Radar

One useful characteristic of the radar is its ability to measure the radial velocity of all objects within the field of view. By exploiting this feature and utilizing static points within the radar's field of view, the ego-vehicle's lateral and longitudinal velocities can be accurately derived through fundamental kinematic relationships.

The Kinematics of Static Points in Relation to the Radar's Radial Velocity

If the radar or ego-vehicle is in motion, reflections from static objects in the field of view will indicate the same velocity as the ego vehicle's velocity but in the opposite direction. Based on this basic kinematic principle, we can derive the ego vehicle's kinematics by utilizing more than one of these static points. The objective is to estimate the longitudinal velocity (v_x), lateral velocity (v_y), and ultimately slip angle (β) of the ego-vehicle using measurements derived from static objects. The schematics are explained in Figure 13, and the relationship between radial velocity (v_r) and angle of arrival (θ) are formulated in Eq. (26).

$$v_r = v_x \cos(\theta) + v_y \sin(\theta) \tag{26}$$

Then this equation is employed to determine v_x and v_y when both v_r and θ are collected from the radar. It is important to note that this formula is applicable only for points obtained from static objects; it does not apply to points from moving objects.

The slip angle β subsequently can be calculated by the following formula (27):

$$\beta = \tan^{-1}\left(\frac{v_y}{v_x}\right) \tag{27}$$

Slip Angle Estimation

When collecting radar data and selecting returns from static points, a large number of static measurements can be obtained; however, not all of them are reliable. Since our system is equipped with GPS, unreliable points can be filtered based on speed information. Specifically, the radar detects both moving vehicles and stationary objects (e.g., trees, walls, traffic lights). According to the kinematic relationship described earlier, radial velocity measurements from stationary objects should remain within the speed range of the ego-vehicle, as radial velocity reflects only the component of the vehicle's motion along the radar's line of sight. Consequently, points with radial velocity values that exceed or fall outside a prescribed range relative to the ego-vehicle's GPS-derived speed are identified as outliers and discarded. This filtering ensures that only physically consistent static points are retained for the slip angle estimation process.

With the filtered data, the following methods are devised and investigated for slip angle estimation.

- Two-Point Median Method: This approach involves selecting two static points from the surroundings, using them to calculate the lateral and longitudinal velocities (v_x and v_y), and then computing the median of all possible combinations of two-point measurements to reduce the impact of outliers.
- Pseudo-Inverse Method: This method leverages all available static points in the scene to estimate v_x and v_y.

For the Two-Point Median Method, two points are selected from the static objects, as expressed in the following Eq. (28).

$$\begin{bmatrix} v_{r_i} \\ v_{r_j} \end{bmatrix} = \begin{bmatrix} cos(\theta_i) & sin(\theta_i) \\ cos(\theta_j) & sin(\theta_j) \end{bmatrix} \begin{bmatrix} v_{x_i} \\ v_{y_j} \end{bmatrix} \tag{28}$$

To enhance robustness against noise and outliers, we formed all possible combinations of static point pairs (i, j), and solved the linear system in (28) for each pair. Then, the median of the resulting v_x and v_y estimates are computed:

$$(\hat{v}_x, \hat{v}_y) = median\left\{\left(v_x^k, v_y^k\right)\right\}_{k=1}^{N} \tag{29}$$

where v_x^k and v_y^k denote the estimated longitudinal and lateral velocities from the k-th point pair, and N is the total number of unique point combinations. This median-based filtering method effectively suppresses the influence of outlier points and yields a more reliable velocity estimate.

On top of that, pseudo-inverse methods can be also explored for estimating the slip angle with collected static points. This method employs all the static points and estimates lateral and longitudinal velocity of the ego-vehicle described in (30).

$$\begin{bmatrix} v_{r_1} \\ \vdots \\ v_{r_n} \end{bmatrix} = \begin{bmatrix} cos(\theta_1) & sin(\theta_1) \\ \vdots & \vdots \\ cos(\theta_n) & sin(\theta_n) \end{bmatrix} \begin{bmatrix} v_x \\ v_y \end{bmatrix} \tag{30}$$

The pseudo inverse of the matrix is then utilized to find v_x and v_y. However, low-cost radar sensors inherently produce multipath reflections and spurious points from surrounding objects, which can result in large peaks in the estimated slip angle from Eqn. (30) [24]. A comparison for one representative scenario is presented in the following sub-section.

Based on the observations from the two aforementioned methods, the filtered data obtained through the median operation is employed for slip angle estimation. This approach mitigates the influence of outliers and spurious radar points, thereby improving the robustness of the estimation.

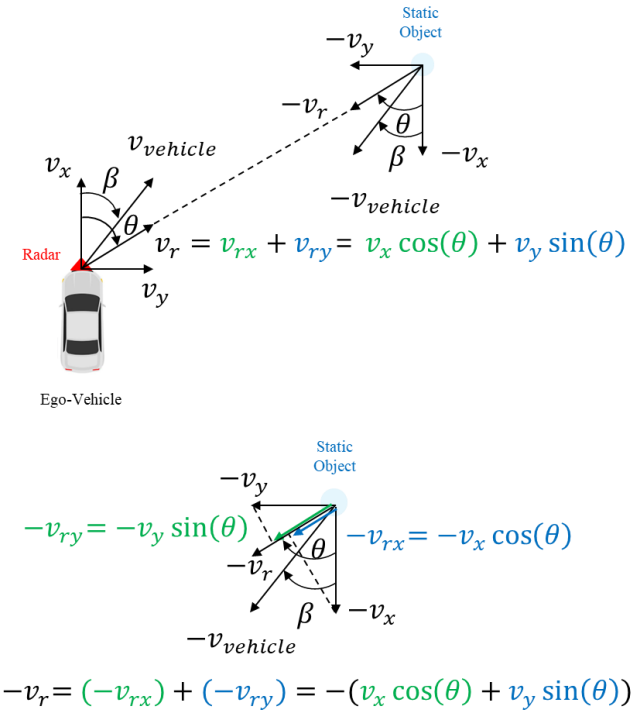

Figure 13: From a blue static target, the radar measures the radial velocity component (v_r) of the relative velocity vector ($v_{vehicle}$).

Comparison Between Proposed Methods

A comparison of the two proposed methods is presented using a sharp-turn scenario described in the following section. In Figure 14, the red and green lines correspond to the two-point median and pseudo-inverse approaches, respectively, while the blue line represents the ground truth obtained from the GPS system. The results indicate that the median method yields smoother estimates with fewer spurious peaks than the pseudo-inverse method, which exhibits larger fluctuations and deviations from the reference trajectory. Moreover, the median-based approach demonstrates greater robustness to outliers and sensor noise, allowing it to capture the underlying

slip angle dynamics more consistently. In contrast, the pseudo-inverse approach is more sensitive to impurities in the radar data, leading to unreliable peaks in the estimation. Based on these observations, the two-point median method is adopted as the preferred approach for estimating the slip angle of the ego-vehicle.

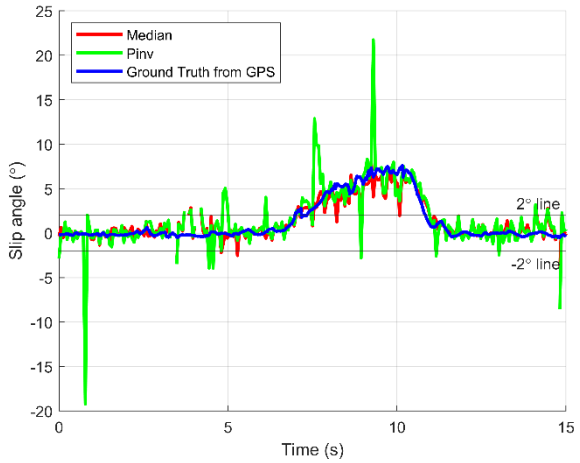

Figure 14: Slip angle estimation: Two-Point Median vs. Pseudo-Inverse methods

5. LIO-SAM: A Framework for Lidar-Based Localization and Mapping

Introduction

LIO-SAM (Lidar Inertial Odometry via Smoothing and Mapping) is a state-of-the-art computational framework for mobile robotics. Developed by Tixiao Shan et al. [11], this system is designed to provide highly accurate, real-time trajectory estimation and map-building for autonomous systems like robots and self-driving vehicles. It achieves this by "tightly coupling" data from two primary sensors: a Lidar (Light Detection and Ranging) and an Inertial Measurement Unit (IMU). The authors claim that this fusion of sensor data allows LIO-SAM to create precise maps and determine a robot's position with minimal drift, even in complex and dynamic environments. Yue et al. [12] demonstrated the application of LIO-SAM for vehicle localization using a factor graph optimization (FGO) architecture, highlighting its robustness and safety in rail transportation GPS denied scenarios.

Core Concepts and Methodology

LIO-SAM operates on a principle known as a factor graph, a mathematical model used to represent and solve complex optimization problems. In this framework, sensor measurements (like Lidar scans and IMU readings) are treated as "factors" that constrain the robot's estimated position and orientation.

1. **Lidar Odometry:** A Lidar sensor measures distances to the surrounding environment by emitting laser pulses and detecting their reflections. LIO-SAM uses this data to perform a process called scan-matching, where it aligns consecutive Lidar scans to estimate how far the robot has moved.

2. **IMU Pre-Integration:** The IMU provides high-frequency measurements of the robot's linear acceleration and angular velocity. LIO-SAM uses a technique called pre-integration to quickly and efficiently estimate the robot's motion between Lidar scans. This provides a robust initial guess for the more computationally intensive Lidar-based odometry.
3. **Tightly-Coupled Fusion:** The genius of LIO-SAM lies in its tight coupling. It doesn't simply use the IMU to correct the Lidar's output. Instead, it integrates both sets of data into a single, unified optimization problem on the factor graph. The IMU data helps "de-skew" the Lidar point clouds (correcting for motion during a scan), and the Lidar data, in turn, helps to correct for the IMU's inherent bias and drift.
4. **Optional GPS Integration:** To further enhance global accuracy, LIO-SAM allows for the optional integration of a GPS signal. This provides an absolute position measurement that can be incorporated into the factor graph as an additional factor, which is especially useful for correcting for long-term drift in large-scale outdoor environments.

System Architecture and Performance

The LIO-SAM system maintains two core factor graphs for optimal performance. One graph handles the real-time odometry and is reset periodically, ensuring a low computational load and a constant output of the robot's immediate position. The second, more comprehensive graph is used for global map optimization, incorporating loop closures (when the robot revisits a previously visited location) and optional GPS measurements to correct for long-term drift and create a globally consistent map. It can process a massive amount of data while maintaining high accuracy, making it suitable for demanding applications in robotics, autonomous navigation, and surveying.

Experimental Results

The LIO-SAM algorithm was implemented and tested using MnCAV data. Although the MnCAV platform is equipped with an RTK-corrected GPS module capable of providing high-precision positioning, GPS availability cannot be guaranteed in all environments. This is especially evident in urban downtown areas with tall buildings, narrow streets, and tree cover, which frequently block or degrade satellite signals.

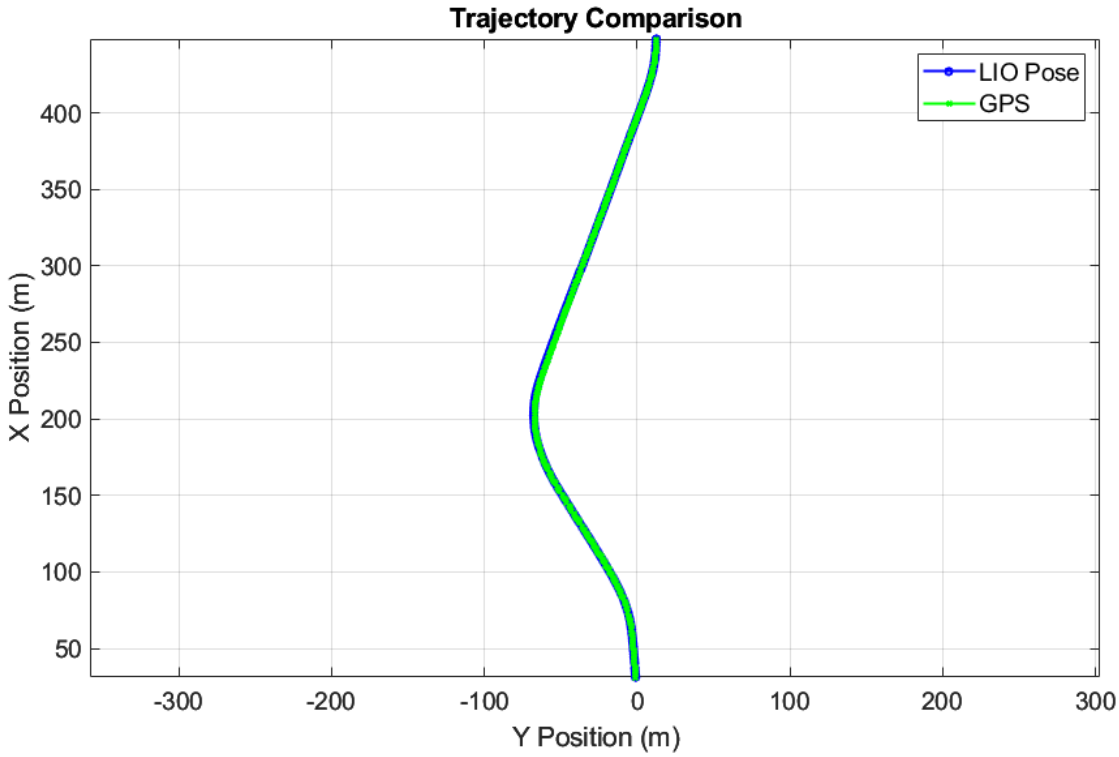

Figure 15: XY plot of MnCAV data

To evaluate LIO-SAM's performance under GPS-denied conditions, the GPS module was manually switched off for a durations of 1, 5 and 10 seconds during vehicle operation and the performance of the algorithm was evaluated. During this interval, the system relied solely on LiDAR and IMU measurements for localization. The preliminary results in Figure 16, Figure 17, Figure 18, Figure 19, Figure 20 and Figure 21 show that LIO-SAM maintained a trajectory drift error of approximately 0.2, 0.5 and 0.8 meters, demonstrating its ability to provide somewhat accurate pose estimation even when GPS data becomes unavailable.

These experiments confirm that LIO-SAM can complement GPS-based navigation and is somewhat capable of handling short-term GPS outages in complex urban environments.

Case 1: 1 second GPS outage

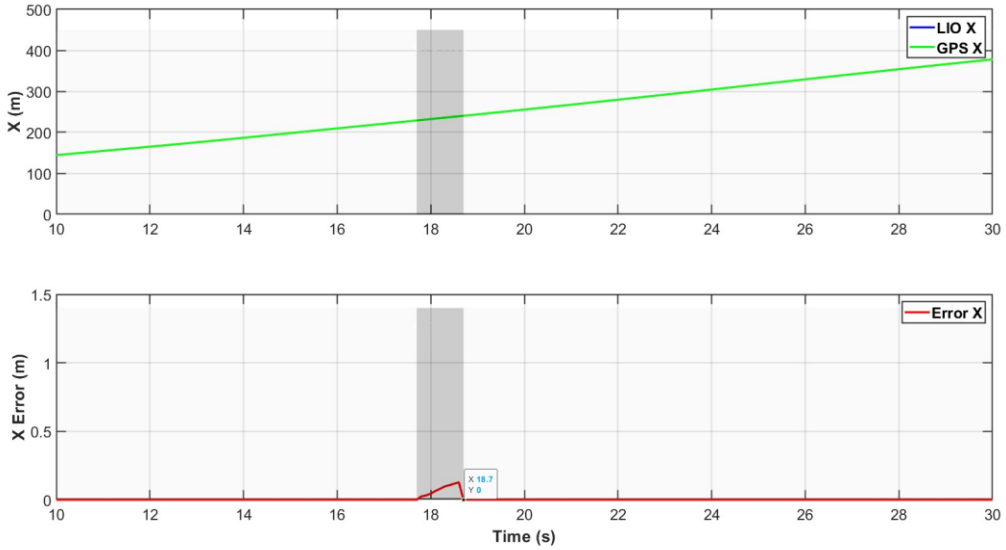

Figure 16: Plot of X position with time (shaded region is gps free region)

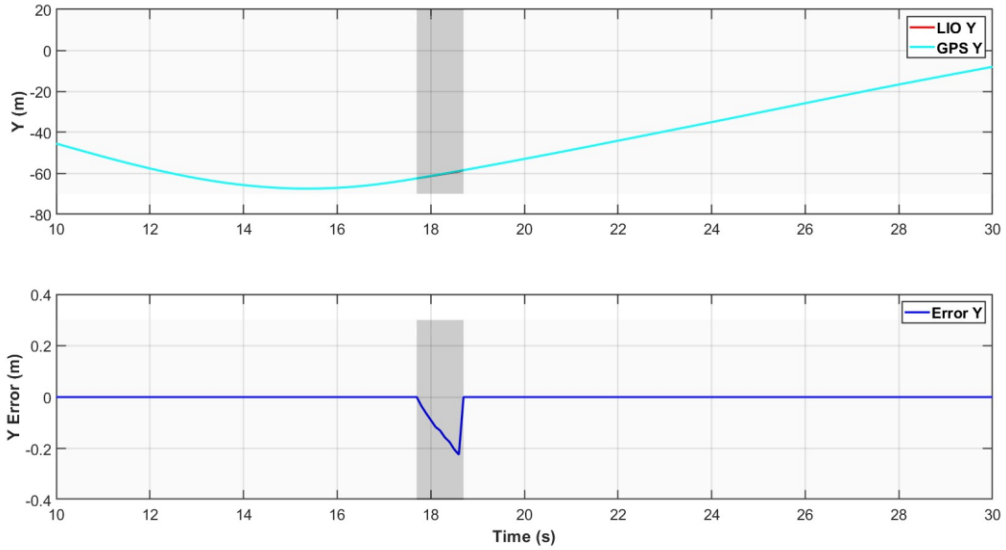

Figure 17: Plot of Y position with time (shaded region is gps free region)

Case 2: 5 second GPS outage

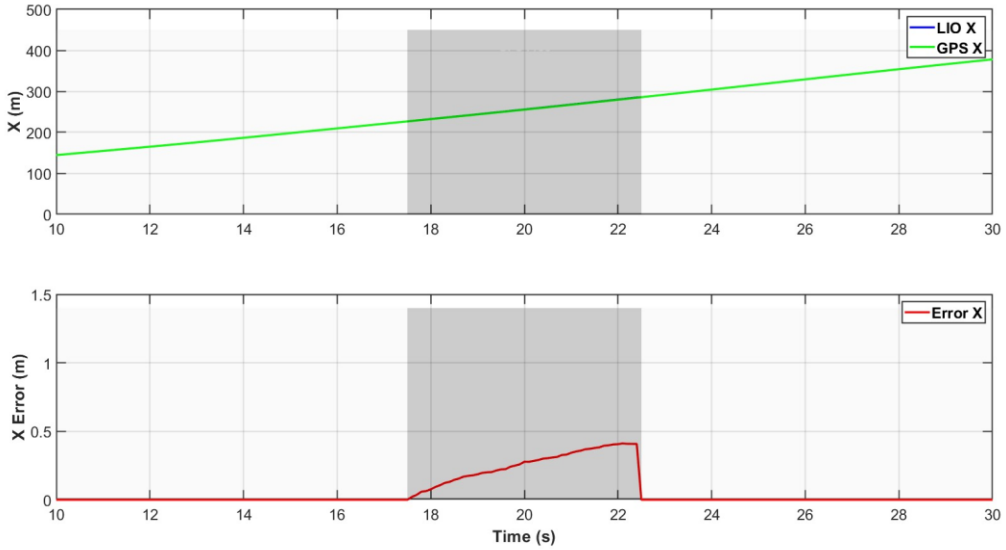

Figure 18: Plot of X position with time (shaded region is gps free region)

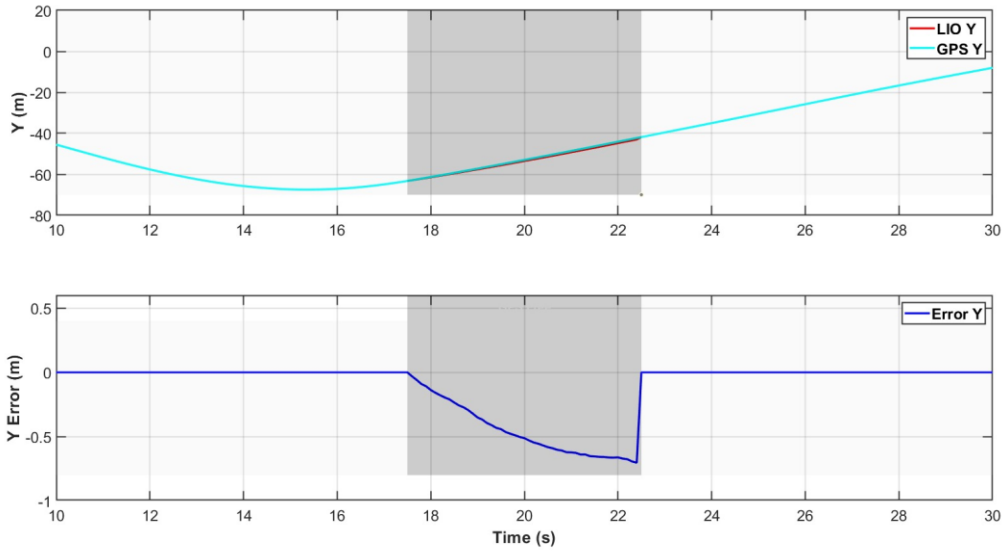

Figure 19: Plot of Y position with time (shaded region is gps free region)

Case 3: 10 second GPS outage

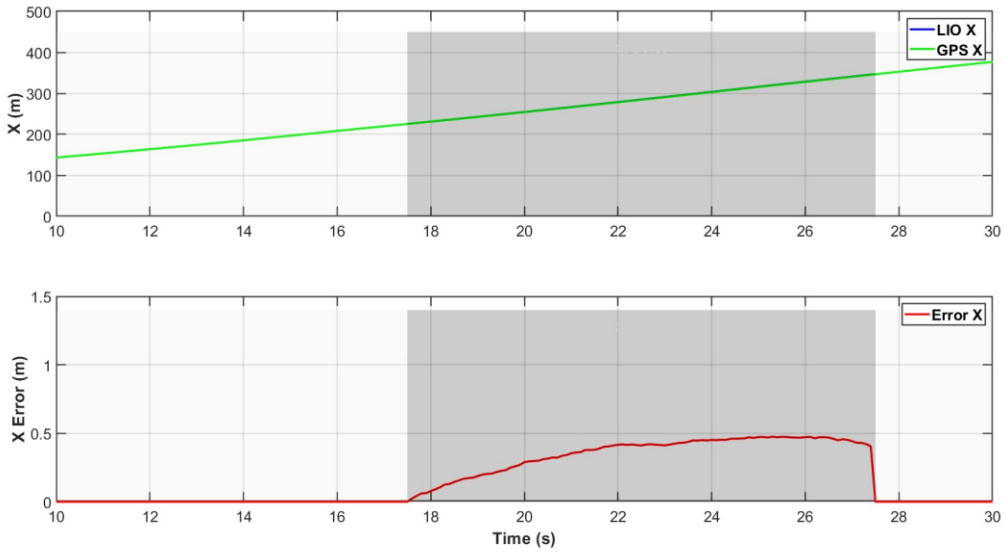

Figure 20: Plot of X position with time (shaded region is gps free region)

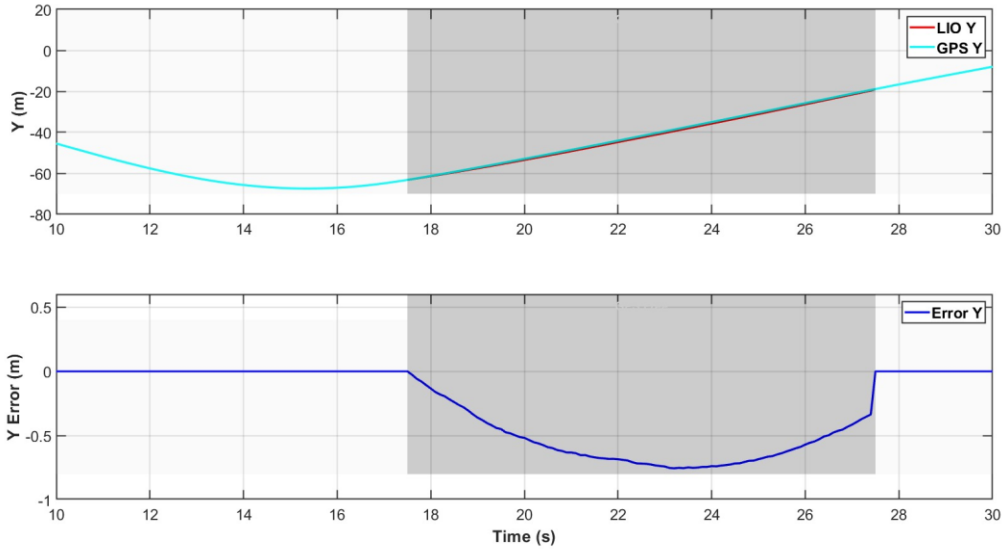

Figure 21: Plot of Y position with time (shaded region is gps free region)

6. Findings

Autonomous vehicles (AVs) have the potential to improve rural road safety. However, low volume rural roads present special challenges for AVs. Such rural roads can be narrow, often will not have right-side lane markers, may not even have center lines, may not be plowed for snow

removal, and can have trees and other objects close to the side of the road. Rural traffic intersections can have missing delineation and signage that are normally provided on higher volume roadways. All of these issues pose major challenges to autonomous driving.

This project specifically looked into solutions for localization on rural roads without the use of cameras so that they can work in the absence of lane markers and/or the presence of snow. The use of RTK-corrected GNSS was explored in detail. A full-scale Chrysler Pacifica MnCAV vehicle at the University of Minnesota was utilized for all data collection. On rural roads without obstructions from trees, RTK-corrected GNSS was found to yield better than 10 cm localization accuracy in terms of standard deviation of error. More than 20 satellites are typically available and used in the position calculation on such roads. However, on roads with dense tree cover, satellite visibility may be completely lost – Data collected on a narrow suburban road with dense trees showed GNSS dropouts lasting several seconds on multiple occasions.

The use of Lidar for localization by utilizing an open-source LIO-SAM algorithm was explored. The LIO-SAM algorithm is a state-of-the-art computational framework that is designed to provide real-time trajectory estimation and map-building for autonomous systems like robots and self-driving vehicles. By using the Lidar sensor to measure distances to the surrounding environment and performing a process called scan-matching, where consecutive Lidar scans are aligned to estimate how far the vehicle has moved between scans, the new location of the vehicle is determined. Analysis of data from the MnCAV vehicle with this algorithm showed that position drifts of approximately 0.2m, 0.5 m and 0.8 m are obtained when GNSS outages occur of 1, 5 and 10 seconds respectively. These results suggest that pre-made maps rather than a SLAM algorithm are needed for reliable localization with Lidar.

Since a dual-antenna GNSS system equipped with a high performance IMU can cost well over $15,000, the feasibility of reliably estimating yaw angle and slip angle without the need for an expensive dual-antenna sensor was studied. Two novel approaches, one based on the use of a high gain observer that utilizes IMU and single-antenna GNSS measurements, and another based on the use of a low-cost radar on the car, were developed. Both approaches showed very good performance with yaw angle and slip angle estimates being within approximately 1 degree of ground truth readings.

The results obtained in this project indicate that a low-cost single-antenna GNSS system can work reliably for localization on rural roads that have at least some open-sky visibility (don’t have dense tree cover).

7. Recommendations

The open skies and low-multipath environments in rural locations can provide significant benefits for AV operations. RTK-corrected GNSS can provide localization accuracy better than 0.1m and can support autonomous steering control as well as intersection identification and handling. GNSS outages due to tree cover can occur in rural environments and will need to be handled. Driving on routes that only involve roads without dense tree cover is a possible solution.

The development of solutions for an autonomous vehicle to safely pass through rural intersections needs to be developed in future work.

8. References

[1] Governors Highway Safety Association (GHSA), “America’s Rural Roads: Beautiful and Deadly,” Sep 2022, Available online at: https://ssti.us/2022/10/10/rural-roads-are-among-americas-most-deadly/

[2] Sun, M., Sun, X., Akter, M., & Ashifur Rahman, M. (2020, May). Crash Risk Factors at Rural Two-Way Stop-Controlled Intersections. In *International Conference on Transportation and Development 2020* (pp. 60-70). Reston, VA: American Society of Civil Engineers.

[3] M. Bertozzi, A. Broggi and A. Fascioli, “Vision-based intelligent vehicles: State of the art and perspectives,” *Robotics and Autonomous systems*, Vol. 32, No. 1, Jul 31, 2000.

[4] L. Alexander and M. Donath, “Differential GPS Based Control of a Heavy Vehicle,” *Proceedings of the IEEE/IEEJ/JSAI International Conference on Intelligent Transportation Systems,* Dates of conference: 05-08 October 1999, DOI: 10.1109/ITSC.1999.821140, 1999.

[5] M. Omae and T. Fujioka, “DGPS-based position measurement and steering control for automatic driving,” *Proceedings of the 1999 American Control Conference*, Dates of Conference: 02-04 June 1999, DOI: 10.1109/ACC.1999.782454, 1999.

[6] S. Patwardhan, H-S. Tan and J. Guldner, “A general framework for automatic steering control: system analysis,” *Proceedings of the 1997 American Control Conference*, Date of Conference: 06-06 June 1997, DOI: 10.1109/ACC.1997.610853, 1997.

[7] R. Rajamani, *Vehicle dynamics and control*, Springer Science & Business Media, ISBN 978-1461414322 2012.

[8] B. Davis and M. Donath, “Development of Sensor Platform for High Accuracy Mapping of Roadway Lane Markings,” *Transportation Research Record*, Vo. 2551, No. 1, 2016.

[9] B. Davis, K. Schwieters, N. Morris and M. Donath, “Deployment of a Snowplow Driver-Assist System,” Report No. MnDOT 2023-27, June 2023.

[10] J.P. Gauthier and I.A. Kupka, “Observability and observers for nonlinear systems,” SIAM journal on control and optimization, 32(4), 975-994, 1994.

[11] T. Shan, B. Englot, D. Meyers, W. Wang, C. Ratti, and D. Rus, “LIO-SAM: Tightly-coupled Lidar Inertial Odometry via Smoothing and Mapping,” *Proc. IEEE/RSJ Int. Conf. Intelligent Robots and Systems (IROS)*, pp. 5135–5142, 2020, doi: 10.1109/IROS45743.2020.9341176.

[12] L. Yue, D. Lu, B. Cai, J. Wang, J. Liu, and W. Jiang, “LIO-SAM for Vehicle Localization Using FGO Architecture,” *2024 International Conference on Electromagnetics in Advanced Applications (ICEAA)*, Lisbon, Portugal, pp. 765–770, doi: 10.1109/ICEAA61917.2024.10701707.

Appendix: Outcomes, Output and Impact

Publications:

- G. Sharma, H. Alai and R. Rajamani, “Simultaneous Ego-Vehicle State Estimation and Vehicle Trajectory Tracking using a Multistage High Gain Observer,” accepted for publication in the journal *Transportation Research – Part C: Emerging Technologies*, October 2025.
- H. Kyong, H. Alai, E.K. Tameh and R. Rajamani, “On the Importance of Slip Angle Estimation for Radar-Based Tracking of Nearby Vehicles,” submitted to the journal *IEEE Transactions on Intelligent Transportation Systems*, under review.

Presentations:

- Rajesh Rajamani, “Interesting ITS Projects in Road Safety,” Safety Working Group, Center for Connected and Automated Transportation, Region 5 UTC, March 22, 2024.
- Rajesh Rajamani, “Autonomous Vehicle Challenges for the US Rural Midwest,” CCAT Global Symposium, March 28, 2025.
- Rajesh Rajamani, “Autonomous Vehicle Challenges for the US Rural Midwest,” Safety Working Group, Center for Connected and Automated Transportation (CCAT), October 24, 2025.

External Funding:

- Minnesota Local Road Research Board and Minnesota Department of Transportation, “Use of MnCORS to Support Autonomous Vehicle Operations in Rural Minnesota,” PI: Rajesh Rajamani, Funding: $178,775, July 1, 2024 – July 31, 2026.
  Objective: This project aims to implement autonomous steering control on the MnCAV vehicle platform using RTK-corrected GNSS and will demonstrate closed-loop control on rural paved roads, gravel roads and on snow-covered roads.